Indian Ocean Dipole modulated wave climate of eastern Arabian Sea

T.R. Anoop[1], V. Sanil Kumar[1]*, P.R.Shanas[1,2], Johnson Glejin[1], M.M. Amrutha[1]

[1]Ocean Engineering Division, CSIR-National Institute of Oceanography (Council of Scientific & Industrial Research), Dona Paula, Goa 403 004 India Tel: 00918322450327, URL: www.nio.org

[2]Ph.D student, Marine physics department, King Abdulaziz University, Jeddah, Saudi Arabia

*Corresponding author: V.S.Kumar, CSIR-National Institute of Oceanography Goa Tel: 0091 832 2450 327 Fax: 0091 832 2450 602 Email: sanil@nio.org

Key points

- Paper investigates the influence of the Indian Ocean Dipole on the wave climate
- Winds from northern Arabian Sea is influenced by Indian Ocean Dipole
- Positive IOD causes decrease of short period waves and vice versa for negative phase
- Variation in wave height during positive/negative IOD due to change in wind direction

Abstract

Intrinsic modes of variability have a significant role in driving the climatic oscillations in the oceanic processes. In this paper, we investigate the influence of an inter-annual mode of variability, the Indian Ocean Dipole (IOD), on the wave climate of the eastern Arabian Sea (AS). Using measured, modeled and reanalysis wave data and reanalysis wind data, we show that the IOD plays a major role in the variability of wave climate of the study region. Due to the IOD induced changes in equatorial sea surface temperature and sea level pressure, the winds from the northern AS gets modified and it produce inter-annual variability in the wave climate over the eastern AS. The change in wind field over the AS due to IOD influence the generation or dissipation of wave field and hence cause the decrease in northwest short period waves during positive IOD and increase during negative IOD.

Key words: surface waves, wave climate, long-term changes, north Indian Ocean, climatic variability

1. Introduction

The north Indian Ocean (IO) is a unique ocean as compared to northern Atlantic and Pacific oceans. Because of the land locked northern boundary, the wind pattern in this region shows semiannual reversal and cause boreal summer (June-September) and winter (December-February) monsoons. Strong westerly in the equatorial IO is limited to short transition periods between the monsoons (both southwest (SW) and northeast (NE)). The equatorial zonal wind reaches maximum around April-May and October-November [Hastenrath and Polzin, 2004]. The wind in eastern Arabian Sea (AS) shows decreasing trend during October and November [Ziegar et al., 2014 (supplementary information)].

Wind waves are the prominent feature of the ocean surface and play a major role in planning activities in the open ocean and in coastal zones [Anoop et al., 2015]. Hence, comprehensive understanding of the properties of the waves and their potential changes are the major knowledge required for sustainable management of both the coastal and offshore region. The wave climate of eastern AS shows large response to seasons and it shows maximum wave height during SW monsoon season [Chempalayil et al., 2012; Glejin et al., 2013a; Kumar et al., 2014; Anoop et al., 2015]. Glejin et al. (2012) analyzed the wave parameters in three locations of eastern AS during SW season and found that the wave height increased from south to north. Shanas and Kumar (2014) studied the changes in wind speed and significant wave height (SWH) in eastern AS by analyzing 34 years data. The average SWH in the eastern AS during pre-monsoon (FMAM), SW monsoon (JJAS) and post-monsoon (ONDJ) are around 1, 2.7 and 0.7 m respectively with an annual average value of ~ 1.1 m [Glejin et al., 2013a]. Apart from seasons, Aboobacker et al. (2011) observed distinct wave characteristics during winter season (NE monsoon and early pre-monsoon) with periodicity ranging from two to five days associated with shamal events in northern AS. Glejin et al. (2013b) also observed the presence of summer shamal swells off Ratnagiri, a location in the eastern AS. The diurnal variation due to sea/land breeze has large influence on the wind-sea climate of eastern AS during the non-monsoon period [Neetu et al. 2006; Glejin et al. 2013a; Amrutha et al., 2016]. Long period southern hemispheric swells are present in eastern AS except during the SW monsoon season [Glejin et al., 2013a].

The monsoon wind patterns in the north IO affect the spatial distribution of sea surface temperature (SST) in the tropical IO. The SST distribution differs from that observed

in Pacific and Atlantic that are warmer on the west [Vinayachandran et al., 2009]. In the IO, warm water is in the eastern side and cold water is in the western side [Vinayachandran et al., 2009]. This SST distribution overturns during the coupled oceanic and atmospheric phenomena in the equatorial IO known as Indian Ocean dipole (IOD) [Saji et al., 1999]. Positive IOD (PIOD) is associated with decreases (increases) of SST and increases (decreases) of sea level pressure (SLP) over the eastern (western) tropical IO. The negative phase of IOD is intensification of the normal condition [Vinayachandran et al., 2009]. In equatorial IO, IOD appears as a dominant contributor of SST variability during the boreal fall season (October-December) [Saji and Yamagatta, 2003]. About 12% of the SST variability in the IO is associated with dipole mode events [Vinayachandran et al., 2009]. There is a phase lag in the SST evolution between the eastern and western tropical IO [Saji et al., 2003] and the regions of positive anomaly (during PIOD) vary with year [Vinayachandran et al., 2009]. The Dipole Mode Index (DMI) is the quantitative representation of strength of IOD and is a measure of the anomalous zonal SST gradient across the equatorial IO. It is defined as the difference between SST anomaly in a western (60°E-80°E, 10°S-10°N) and an eastern (90°E-110°E, 10°S-0°S) box. Seasonal phase locking is the important characteristic of the DMI time series. It is moderately correlated with nino3 (ENSO) index, but it is strongly correlated with equatorial winds over the IO [Saji et al., 1999]. Monthly DMI are available in the website of Japan Agency of Marine-Earth Science and Technology (www.jamstec.go.jp).

The tropical IO displays strong inter-annual climate variability associated with the El Niño–Southern Oscillation (ENSO) and IOD [Murtugudde et al., 2000; Slingo and Annamalai, 2000]. Baquero-Bernal et al. [2002] found that IOD shows good correlation with ENSO in the equatorial Pacific Ocean. However, the correlation between the strength of ENSO and IOD are not linear [Shinoda and Han, 2005]. IOD co-occurring with ENSO are forced by a zonal wind shift in the descending branch of Walker circulation in the eastern IO and the process that initiate IOD in the absence of ENSO are not clear [Vinayachandran et al., 2009].

The impact of IOD on the wind pattern in the equatorial IO is examined in the following studies. SST and SLP variation produced by IOD cause easterly zonal wind anomaly especially in its zonal component in equatorial IO [Reverdin, 1985; Murtugudde et al., 2000; Saji et al., 1999; Webster et al., 1999; Sreenivas et al., 2012]. The IOD forced wind anomalies are maximum in the central equatorial IO [Sreenivas et al., 2012] and the

significant anomalies appear around June, intensify in the following months and peaks at October. The anomalous easterlies weaken the eastward Wyrtki jets [Wyrtki, 1971] in the equatorial IO [Reverdin, 1985]. The wind anomaly produced during IOD has longer duration, but ENSO has shorter duration [Rao et al., 2002].

Even though the influence of IOD on the wind pattern of IO is reported [Saji et al., 1999], the role of this event on the wave climate of IO is not yet studied. Glejin et al. [2013c] pointed out the possibility of influence of IOD on the wave climate of southeast coast of India, but further analysis on this topic in this region is not carried out. Most of the studies in the past have focused on the influence of IOD on the wind pattern of equatorial IO. In this paper, we have examined the impact of IOD on the surface wind field of AS and its impact on the wave climate of eastern AS. The analysis is confined to October, when the impact of the IOD is strongest and wind conditions in the AS are calmest. Fig. 1a shows the study area. The data sets used in this study and the details of the numerical models are described in section 2. Section 3 describes results and discussion, and the main findings are summarized in section 4.

2. Data and methods

The major challenge for the wave climate study in eastern AS is the scarcity of long-term observational data. Here, in the present study we used the available measured data using Datawell directional waverider buoy off Ratnagiri (available from 2010 to 2014) and off Honnavar (available from 2008 to 2014) off central west coast of India. Among these, Ratnagiri is the northern and Honnavar is the southern location and these locations are spaced at ~ 350 km apart. The details of the data analysis are similar to that presented in Kumar et al. [2014]. The spectral climatology of the study area is presented by Kumar and Anjali [2015].

Due to scarcity of sufficient measured data, we used reanalysis product of ECMWF (European Centre for Medium-Range Weather Forecasts) i) ERA-40 [Uppala et al., 2005] for the period 1958 to 1978 and ii) ERA-I [Dee et al., 2011] for the period 1979 to 2014 for deriving the wind climatology. Spatial resolution of ERA-40 is 1.5º X 1.5º and ERA-I is 1° X 1°. Performance of ERA-I was previously evaluated over tropical and north IO and showed good performance compared with observation for wind and wave [Kumar et al., 2013; Shanas and Kumar, 2014; Kumar and Naseef, 2015]. In the present study, blended data sets of ERA-

40 and ERA-I is used only for long-term wind field analysis during positive, negative and neutral IOD years. Since ERA-I is the improved version of ERA-40 [Dee et al., 2011], we compared the ERA-40 with ERA-I during October from 1979 to 2001 (Fig. 2). From the analysis, it is clear that the error in ERA-40 compared to ERA-I will not significantly affect the results when we blend these datasets together. For SST data we used the daily averaged Tropflux SST with 1º X 1º resolution from 1979 to 2014 [Kumar et al., 2012].

In order to simulate the directional wave spectrum at the buoy location, we have used two third-generation spectral wave models; WAVEWATCH III (WW3) 4.18 and Simulating Waves Nearshore (SWAN) 41.01. WW3 is the wave model developed by NOAA/ NCEP [Tolman, 1991; 2009] and is based on finite difference solving of the energy balance equation of the spectral wave action in the approximation of phase averaging. The coastal wave model SWAN is a third-generation, phase averaged numerical wave model for the simulation of waves in waters of deep, intermediate and finite depth [Booij et al., 1999]. The physical parameterization of model physics of WW3 is described in several works [e.g. Tolman, 1991; 2009] and that for SWAN by Booij et al. [1999], Ris et al. [1999] and Bunney [2011]. We have implemented a coarse resolution WW3 model with a resolution of 0.25^{o} x 0.25^{o} in latitude and longitude covering the entire domain in the IO (20^{o} E-78^{o} E and 70^{o} S - 35^{o} N) and a SWAN model with relatively finer grid of 1 minute in the NIO (70-75^{o} E and 10-20^{0} N). We used high-resolution bathymetry from the 1-minute gridded elevations/bathymetry for the world (ETOPO1) database [Amante and Eakins, 2009] available from the National Geophysical Data Centre (NGDC, United States).

Wave frequencies were discretized over 25 bins on a logarithmic scale from 0.04 to 1 Hz; wave direction was binned into 36 intervals of 10° each. WW3 run carried out using physical processes contained in source term package-2 (ST2) [Tolman and Chalikov, 1996]. The terms selected are bottom friction and depth-induced breaking [Hasselmann et al., 1973]. The wind growth and white capping [Komen et al., 1984], quadruplet and triad interaction processes were activated. The WW3 model is driven by the surface wind fields from ERA-I at every 6 h interval and the time series 2-dimensional energy density spectra obtained is used as the boundary condition for the higher-resolution nearshore wave model SWAN. For comparison of the SWH estimated in deep water using WW3, the measured wave data collected using a moored Seatex buoy (Oceanor, Norway) under the National Data Buoy Programme [Premkumar et al., 2000] at AS2 location in the AS (15.00° N; 69.00° E; water

depth ~ 3000 m) during October 2009 is used. The heave data of the buoy is recorded at 2 Hz interval for 17 minutes duration and from the recorded heave data, the wave spectrum is obtained through fast Fourier Transform and the SWH is estimated from the zeroth spectral moment (m_o) as SWH= $4\sqrt{m_o}$. For quantitative comparison between measured and model output, several error statistics have been determined; Pearson's linear correlation coefficient r, root-mean-square (RMS) error, bias, and scatter index (SI). The comparison of model results with measured data in deep water is carried out only for October 2009, since our study is only on the influence of IOD on the wave climate during October. But for shallow water area (Ratnagiri) which is our area of interest we carried out validation for 2011 September to November (Fig. 3). From this it is found that for shallow and deep water both models show 0.95 correlation. Whereas for deep water the model is slightly underestimating (-0.13 m) and for shallow water it is overestimating (0.06 m). Scatter index and RMSE error of both models are very small. From this we can see that the model shows good performance in both deep and shallow water areas.

3. Results and discussion

During October and November, the waves in the AS are dominated by low-amplitude (SWH < 1 m) wind-seas [Young, 1994, Chempalayil et al., 2012, Glejin et al., 2013a], and during this time the DMI reaches its maximum value. For this particular period we examined the role of DMI on the wave climate of eastern AS and observed that during October surface waves in this region shows response to DMI. We selected six locations (Fig. 1a) along the eastern AS which are at more than 100 km away from the coast of India (Table 1). The time series plot of SWH and mean wave period (MWP) with DMI are shown in Fig. 4a. Correlation and partial correlation of the wave parameters with DMI and SOI (southern oscillation index) are shown in Table 1 and it shows that SWH is negatively related and MWP is positively related to DMI. The influence of IOD increases towards south, but after removing ENSO (SOI) the correlation values in all locations decreases and maximum correlation is observed in the central AS (location L4). This implies that if influences of ENSO are removed, then IOD have more impact on the central eastern AS. Impact of ENSO with and without IOD is checked here and identified that without IOD, the impact of ENSO is significant only in the southern part of eastern AS. From this it is certain that in the eastern AS region IOD has more impact than ENSO and its effect is dominant off the central west

coast of India. Variability of SWH and MWP with respect to DMI index from 1979 to 2013 is shown in time series plot at the same six locations (Fig. 4a). The anomaly in the SWH varies between -0.2 m and 0.4 m and that for MWP from -2 s to 1 s. Maximum SWH and MWP anomaly is observed during 1997, which is the strongest IOD year for the study period.

The composite climatology (using ERA-40 and ERA-I) of October wind pattern (from 1958 to 2014) of AS and a part of equatorial IO is shown in Fig. 1b. The wave measuring locations (Ratnagiri and Honnavar) in central eastern AS is shown as red dots (Fig. 1a). The eastern AS region shows comparatively strong wind compared to the western AS. The wind from the northern AS passes parallel to the Indian west coast to eastern equatorial IO after merging with equatorial westerly, while over the central AS the wind vectors are from northerly direction and change their direction to north-westerly before merging with the westerly equatorial winds and north-westerly winds nearer the Indian coast. This pattern of wind is due to the low pressure in the eastern equatorial IO due to the warm water in this region compared to western equatorial IO [Vinayachandran et al., 2009].

Pure positive IOD and combined events are considered following Aparna et al. [2012]. A pure IOD event is that which occurred in the absence of an ENSO event [Rao et al., 2002]. A positive (negative) IOD event that co-occurred with an El Niño (La Nina) is a combined IOD event. A pure ENSO event is defined similarly. The combined events are to be strong only if both El Niño and positive IOD events are strong. Figures 1c and 1d are the wind pattern during pure positive and combined IOD events respectively. As observed from climatology, these figures illustrate that in the eastern AS the north-westerly wind vectors are modified to north-easterly. Instead of going to eastern equatorial IO the wind blows to western IO. This can be perceived as more strong in combined event of PIOD with a comparatively weak wind vectors along the southwest of India. During the negative IOD (NIOD) events (Figs. 1e and 1f) wind blows over the central and eastern AS as north-westerly which is in contrast to the wind pattern during PIOD. This modification in the wind pattern over the central AS to either westward or eastward direction from its general climatology pattern during the PIOD or NIOD events is due to the IOD induced temperature variability in the equatorial IO.

Measured frequency-directional spectrum of surface waves from two locations off the central west coast of India are shown in Fig. 5. The wind pattern of corresponding years is

shown in Fig. 5a and year wise SST anomaly in west, east and DMI index for October is shown in Fig. 4a and 4b. For the years 2008 to 2014, it can be seen that maximum positive DMI index is observed during 2011 (Fig. 4a). During this year the winds in eastern AS has shifted its direction as north-easterly. Its influence is clearly visible in the frequency-directional spectrum of waves at Ratnagiri and Honnavar, due to the decrease in short period waves from northwest (NW) direction. This difference in higher energy at Ratnagiri than Honnavar is clearly evident from Figures 5b &5c and is caused by the alteration of wind direction to NE before reaching Honnavar. So the dissipation of NW waves and weak wind at Honnavar region causes decrease in the short period wave energy. Similar patterns are observed in other years such as 2008, 2012 and 2014 which has got comparatively higher DMI. Endo and Tozuka (2015) classified 2008 as IOD Modoki, 2011 and 2012 as Canonical IOD years and hence higher DMI is observed in these years.

In contrast to the above, the only year with negative DMI during 2008 to 2014 is in 2010. During 2010, the wind pattern is in NW direction and dominance of short waves from NW is higher. Similar pattern can be seen in 2009 and 2013 as these years also have low DMI index. Unlike PIOD, during negative IOD, the short period waves are slightly higher at Ratnagiri than at Honnavar and this may be due to the dissipation of the waves from NW due to the larger distance travelled by the waves to reach Honnavar than Ratnagiri. From Figure 4b we can see that maximum positive anomaly in SST of western equatorial IO since 2008 is observed in 2009. However, the influences of high SST anomalies are not observed either in the wind pattern or wave climate. This depicts that the modification of wind vectors not only depends on the SST anomaly in the west or east separately but also on the DMI index.

To confirm the influence of IOD induced turning wind pattern (Fig. 1b to 1f) on the waves off the west coast of India, we spatial averaged the zonal wind component within the region where wind shows alteration in its direction (14°N to 20°N; 70°E to 73°E) and averaged the short period waves within 0.14 Hz to 0.29 Hz frequency and 280º-320º direction. The scatter plot for both zonal wind and measured SWH in this particular direction and frequency range off Ratnagiri and off Honnavar for all years are shown in Figure 6. From the figure it can be seen that the zonal wind component in this region has a direct influence to the wave climate of this region. SWH increases with the zonal wind component, and this increase is greater when the zonal wind component is positive than when it is negative.

During the negative phase of IOD, the swell height is slightly less than that during the positive phase (Figures 5b and 5c). The turbulent sea state generated by dominance of short period waves during negative phase of IOD, leads to increased decay rate of swell [Ardhuin et al., 2009; Young et al., 2013]. The sign reversal of the air-sea momentum flux depends on a parameter known as inverse wave age (ratio of sea surface wind speed to the speed of the wave corresponding to peak frequency) and it is very useful to understand the present sea state [Grachev and Fairall, 2001; Hanley and Belcher, 2008; Hanley et al., 2010]. Here, we calculated the monthly (October) average inverse wave age off Ratnagiri and the values are 0.32, 0.11, 0.27, 0.35 and 0.17 from 2010 to 2014. From this it is more evident that during the positive phase of IOD, the eastern AS is a wave-driven wind region (inverse wave age < 0.15), i.e. waves transfer momentum to wind. During the negative IOD period, region becomes mixed state (0.15 < inverse wave age < 0.83; both wind driven wave and wave driven wind are present). The modelled frequency-directional spectrum off Ratnagiri and Honnavar from 2010 to 2014 is shown in figures 5d and 5e. Comparison of measured and modelled spectra off Honnavar and Ratnagiri shows that the spectral energy is overestimated by the model since the ERA-I wind data used in the study is with a coarse resolution of 1° x 1° (Fig. 5b and 5c). Even though the model overestimated the spectral energy, it can be observed that the model reproduced almost the same pattern as observed wave spectra. The influence of altering wind pattern is clearly evident in the modelled spectra as well.

Since IOD has large influence on SST variability in equatorial IO, here we show the SST of AS and western equatorial Indian Ocean in Figure 7. Here, we considered comparatively strong PIOD and NIOD events from 1979 to 2014. The PIOD years are 1982, 1994, 1997 and 2006 (left panel of Fig. 7). Among these in 1994, IOD occurs in the absence of ENSO. The NIOD years are 1980, 1984, 1996 and 1998 (right panel). This SST variability produces variability in SLP (Fig. 8). The wind pattern of the respective years for AS and part of equatorial IO are shown in same figure. Since the NIOD is the intensification of the normal condition of October [Vinayachandran et al., 2009], the SLP in western equatorial IO is higher and lower in eastern equatorial IO. Hence, the winds from the northern AS will propagate towards eastern equatorial IO along eastern AS. This is the influence of IOD induced temperature variability on SLP and wind direction.

Since the performance of numerical model is good we have carried out further analysis using this model for the period where measured data is not available. Simulated

directional spectra for the years 1980, 1982, 1984, 1994, 1996, 1997, 1998 and 2006 are shown in Figure 9. Column one and three are for PIOD years off Ratnagiri and off Honnavar respectively, similarly column 2 and 4 are for NIOD years. From the figure it is evident that for the positive phase of IOD, the short period waves from the NW direction is less at both locations, whereas in 2006 it shows a conflicting result. From Figure 8, it is clear that in 2006 the wind pattern in the central AS is north-easterly as observed in the other PIOD events, but along the eastern AS wind vector are slightly extended southerly compared to the strong events observed during 1994 and 1997. Similar pattern, but comparatively less spatial extension in wind vectors towards south is also evident during 1982 (Fig. 8).

In case of 1996, which is the strongest NIOD events considered for this study, we expect a more evident signature in SWH at the study locations: Ratnagiri and Honnavar. However, in the wave spectrum its signature is weaker than that observed in 1980 and 1984 (Fig. 9). Wind pattern observed during the period, in 1996, is northerly down to 15^{o} N then it turns as north-westerly and propagates towards eastern equatorial IO (Fig. 8). The change in wind pattern from the composite climatology of NIOD events (Fig. 1e & 1f) cause the weakening of short period waves arriving from the NW and corresponding influence in directional wave spectra. Similarly, the second strongest NIOD events occurred in 1998, but the signature of this event is absent on the wave climate. The northern-eastern AS region is calm due to the absence of NW winds in the northern AS, in turn due to the associated negative SLP anomaly.

4. Conclusions

We analysed the wind pattern over the AS and examined the influence of IOD events on the wave climate of eastern Arabian Sea using reanalysis, observation, and model datasets. Analysis of wind pattern influenced by the IOD has been carried out by removing the influence of ENSO from IOD and vice versa. It has been found that IOD has significant influence on the wave climate off the central west coast of India compared to the northern and southern parts. The decreasing of wave height during PIOD is due to the decrease of short period waves from northwest direction. Wind blowing from the northern AS is the major determining factor on wave climate. In general, climatology of wind pattern in central and eastern AS during October is northerly and north-westerly respectively. During PIOD events, wind vectors modify its direction and blow as north-easterly because of the IOD

induced SST anomaly in the equatorial Indian Ocean. This brings a weakening of wind field over the central and south of central west coast of India. This change in direction of wind pattern in AS cause the decrease in wave height off central and south west coast of India during PIOD. Whereas, during NIOD events wind vectors turn to north-westerly instead of northerly winds in the composite climatology over the region during October. It leads to increasing of short period waves in same region. The influence of IOD on the wave climate mainly depends on the modification of wind field caused by the phases of IOD event. If this wind pattern is absent even during strong IOD event, then the signature of IOD on the wave climate is also absent. This alteration of wind pattern mainly depends on the IOD induced SST variability in eastern and western equatorial IO and some other unknown factors may also cause slight modification in this wind which requires more analysis to understand this variability. From this study it is clear that IOD has an impact on the wave climate off west coast of India especially off the central west coast of India due to the decrease of north-westerly short period waves.

Acknowledgements

Authors acknowledge the CSIR, New Delhi for funding the wave measurement at Honnavar and ESSO- INCOIS, Ministry of Earth Sciences, Government of India for funding the wave measurement at Ratnagiri. The director CSIR-NIO, Goa provided encouragement to carry out the study. The deep water buoy data used for validation of numerical model was collected by National Institute of Ocean Technology, Chennai and provided by Indian National Centre for Ocean Information Services (INCOIS) Ministry of Earth Sciences, Hyderabad. Dr. T. M. Balakrishnan Nair, Mr. Arun Nherakkol and Mr. Jai Singh provided support during data collection. We thank Dr. Vedpathak and Mr. Parag Kulkarni, Centre for Coastal & Marine Biodiversity, Dr. Babasaheb Ambedkar Marathwada University, Ratnagiri for providing the logistics required for wave data collection at Ratnagiri. This work forms part of the Ph.D. thesis of the first author. We thank the topic editor Dr. John M. Huthnance and the two reviewers for the critical review and the suggestions, which improved the scientific content of the paper. This work is NIO contribution No. 2015.

References

Ardhuin, F., Chapron, B., and Collard, F.: Observation of swell dissipation across oceans, Geophys. Res. Lett., 36, L06607, doi:10.1029/2008GL037030, 2009.

Aboobacker, V. M., Rashmi, R., Vethamony, P., and Menon, H. B.: On the dominance of pre-existing swells over wind seas along the west coast of India, Cont. Shelf Res., 31(16), 1701-1712, 2011.

Amante, C. and Eakins, B. W.: ETOPO1 1 arc-minute global relief model: procedures, data sources and analysis, NOAA Tech. Memo., NESDIS NGDC-24, National Oceanic and Atmospheric Administration, Boulder, Colorado, USA., 19 pp., 2009.

Amrutha, M.M., Kumar, V.S. and Singh, J.: Changes in nearshore waves during the active sea/land breeze period off Vengurla, central west coast of India, Annales Geophysicae (in press), 2016.

Anoop, T.R., Kumar, V.S., Shanas, P.R., and Johnson, G.: Surface wave climatology and its variability in the North Indian Ocean based on ERA-Interim reanalysis. Journal of Atmospheric and Oceanic Technology, 32, 1372-1385. doi: 10.1175/JTECH-D-14-00212.1, 2015.

Aparna, S. G., McCreary, J. P., Shankar, D., and Vinayachandran, P. N.: Signatures of Indian Ocean Dipole and El Niño–Southern Oscillation events in sea level variations in the Bay of Bengal, J. Geophys. Res.-Oceans., 117, C10012, 2012. DOI: 10.1029/2012JC008055.

Baquero-Bernal, A., Latif, M., and Legutke S.: On dipole like variability of sea surface temperature in the tropical Indian Ocean, J. Clim., 15(11), 1358-1368, 2002.

Booij, N., Ris, R. C., and Holthuijsen L. H.: A third-generation wave model for coastal regions: 1. Model description and validation, J. Geophys. Res. Oceans.,104(C4), 7649-7666. 1999..

Bunney, C.: A high resolution SWAN model assessment: North Norfolk to Humber. Forecasting Research Technical Report 557, Met Office, Devon, United Kingdom, 2011.

Chempalayil, S. P., Kumar, V. S., Johnson, G., Udhaba, D. G., and Vinayaraj, P.: Interannual and seasonal variations in nearshore wave characteristics off Honnavar, west coast of India, Curr. Sci., 103, 286–292, 2012.

366 Dee, D. P., Uppala, S. M., Simmons, A. J., Berrisford, P., Poli, P., Kobayashi, S., ... and
367 Vitart F.: The ERA-Interim reanalysis: Configuration and performance of the data
368 assimilation system, Q. J. R. Meteorolog. Soc., 137(656), 553-597, 2011.

369 Endo, S., and Tozuka, T.: Two flavors of Indian Ocean Dipole. Climate. Dyn., 1-15, 2015.

370 Grachev, A. A., and Fairall, C. W.: Upward momentum transfer in the marine boundary
371 layer, J. Phys. Oceanogr., 31, 1698–1711, 2001.

372 Hanley, K. E., and Belcher, S. E.: Wave-driven wind jets in the marine atmospheric boundary
373 layer, J. Atmos. Sci., 65, 2646–2660, 2008.

374 Hanley, K E., Belcher, S. E., and Sullivan, P. P.: A global climatology of wind-wave
375 interaction, J. Phys. Oceanogr., 40(6), 1263-1282, 2010.

376 Glejin, J., Kumar, V.S., Sajiv, P.C., Singh, J., Pednekar, P., Kumar, K.A., Dora, G.U., and
377 Gowthaman, R.: Variations in swells along eastern Arabian Sea during the summer monsoon,
378 Open J. Mar. Sci., 2 (2), 43–50, 2012.

379 Glejin, J., Kumar, V. S., Nair, T. B., and Singh J.: Influence of winds on temporally varying
380 short and long period gravity waves in the near shore regions of the eastern Arabian
381 Sea, Ocean Sci., 9, 343-353, 2013a.

382 Glejin, J., Kumar, V. S., Nair, T. B., Singh, J., and Mehra P.: Observational Evidence of
383 Summer Shamal Swells along the West Coast of India, J. Atmos. Oceanic Technol., 30(2),
384 379-388, 2013b.

385 Glejin, J., Kumar, V. S., and Nair T. M. B.: Monsoon and cyclone induced wave climate over
386 the near shore waters off Puduchery, south western Bay of Bengal, Ocean Eng., 72, 277-286,
387 2013c.

388 Hasselmann, K., Barnett, T.P., Bouws, E., Carlson, H., Cartwright, D.E., Enke, K., Ewing,
389 J.A., Gienapp, H., Hasselmann, D.E., Kruseman, P., Meerburg, A., Mu¨ ller, P., Olbers, D.J.,
390 Richter, K., Sell, W., and Walden H.: Measurements of wind-wave growth and swell decay
391 during the Joint North Sea Wave Project (JONSWAP). Deutsche Hydrographische Zeitschri
392 Supplement A., 8(12) 95p, 1973.

Hastenrath, S., and Polzin D.: Dynamics of the surface wind field over the equatorial Indian Ocean, Q. J. R. Meteorolog. Soc., 130 (597), 503-517, 2004.

Komen, G., Hasselmann, S., and Hasselmann K.: On the existence of a fully developed wind-sea spectrum, J. Phys. Oceanogr., 14(8), 1271–1285, 1984.

Kumar, B. P., Vialard, J., Lengaigne, M., Murty, V. S. N., McPhaden, M. J., Cronin, M. F., Pinsard, F., and Reddy K. G.: TropFlux wind stresses over the tropical oceans: evaluation and comparison with other products, Clim. Dyn., 40, 2049-2071, 2013.

Kumar, B. P., Vialard, J., Lengaigne, M., Murty, V. S. N., and McPhaden M. J.: TropFlux: air-sea fluxes for the global tropical oceans-description and evaluation, Clim. Dyn., 38(7-8), 1521-1543, 2012.

Kumar, V. S., Shanas, P. R., and Dubhashi K. K.: Shallow water wave spectral characteristics along the eastern Arabian Sea, Nat. Hazard., 70(1), 377-394, 2014.

Kumar, V. S., and Naseef T. M.: Performance of ERA-Interim wave data in the nearshore waters around India. J. Atmos. Oceanic. Technol., 32(6), 1257-1269, 2015.

Kumar, V. S., and Anjali N. M.: Inter-annual variations in wave spectral characteristics at a location off the central west coast of India, Annales Geophysicae., 33, 159-167, 2015.

Murtugudde, R., McCreary, J. P., and Busalacchi A. J.: Oceanic processes associated with anomalous events in the Indian Ocean with relevance to 1997–1998, J. Geophys. Res. Oceans., 105, 3295–3306, 2000.

Neetu, S., Shetye, S. R., and Chandramohan P.: Impact of sea breeze on wind-seas off Goa, west coast of India, J. Earth Syst. Sci.,115(2), 229-234, 2006.

Premkumar, K., Ravichandran, M., Kalsi, S. R., Sengupta, D., and Gadgil S.: First results from a new observational system over the Indian Seas. Curr Sci**.,** 78, 323-330. (2000),

Rao, A. S., Behera, S. K., Masumoto, Y., and Yamagata T.: Interannual subsurface variability in the tropical Indian Ocean with a special emphasis on the Indian Ocean Dipole, Deep Sea Res, Part II., 49, 1549–1572, 2002.

Reverdin, G.: Convergence in the equatorial surface jets of the Indian Ocean, J. Geophys. Res. Oceans., 90, C6, 11741-11750, 1985.

Ris, R.C., Holthuijsen, L.H., and Booij N.: A third-generation wave model for coastal regions 2. Verification, J. Geophys. Res. Oceans, 104 (4), 7667-7681. 1999.

Saji, N. H., and Yamagata T.: Structure of SST and Surface Wind Variability during Indian Ocean Dipole Mode Events: COADS Observations, J. Clim., 16(16), 2735-2751, 2003.

Saji, N. H., Goswami, B. N., Vinayachandran, P. N., and Yamagata T.: A dipole mode in the tropical Indian Ocean, Nature, 401, 360–363, 1999.

Shanas, P. R., and Kumar V. S.: Temporal variations in the wind and wave climate at a location in the eastern Arabian Sea based on ERA-Interim reanalysis data, Nat. Hazards Earth Syst. Sci., 14(5), 1371-1381, 2014.

Shinoda T., and Han W.: Influence of the Indian Ocean dipole on atmospheric sub seasonal variability, J. Clim., 18 3891 3909, 2005.

Slingo, J. M., and Annamalai, H.: The El Nino of the century and the response of the Indian summer monsoon, Mon. Weather Rev., 128, 1778–1797, 2000.

Sreenivas, P., Gnanaseelan C., and Prasad K. V. S. R.: Influence of El Niño and Indian Ocean Dipole on sea level variability in the Bay of Bengal, Global Planet. Change., 80, 215-225, 2012.

Tolman, H. L.: User manual and system documentation of WAVEWATCH III TM version 3.14. Tech. Note., 276, National Oceanic and Atmospheric Administration, National Weather Service, Maryland, USA 194 pp., 2009.

Tolman, H. L.: A third-generation model for wind waves on slowly varying, unsteady and inhomogeneous depths and currents, J. Phys.Oceanogr., 21, 782–797, 1991.

Tolman, H.L., and Chalikov, D.: Source terms in a third-generation wind wave model. J. Phys. Oceanogr., 26, 2497-2518, 1996.

Uppala, S. M., Kållberg, P. W., Simmons, A. J., Andrae, U., Bechtold, V., Fiorino, M., and Woollen J.: The ERA-40 re-analysis, Q. J. Roy. Meteor Soc., 131(612), 2961-3012, 2005.

Vinayachandran, P. N., Francis, P. A., and Rao, S. A.: Indian Ocean dipole: processes and impacts, Current Trends in Science: Platinum Jubilee Special, Indian Academy of Sciences Bangalore, 569-589, 2009.

Webster, P. J., Moore, A. M., Loschnigg, J. P., and Leben R. R.: The great Indian Ocean warming of 1997-1998: Evidence of coupled oceanic-atmospheric instabilities, Nature., 401(6751), 356-360, 1999.

Wyrtki, K.: Oceanographic Atlas of the International Indian Ocean Expedition, 531 pp., Natl. Sci. Found., Washington, D. C, 1971.

Young, I. R.: Global ocean wave statistics obtained from satellite observations, Appl. Ocean. Res., 16.4, 235-248, 1994.

Young, I.R., Babanin, A.V., and Zieger, S.: The decay rate of ocean swell observed by altimeter, J. Phys. Oceanogr., 43, 2322-2333, 2013.

Zieger, S., Babanin, A.V., and Young, I.R.: Changes in ocean surface winds with a focus on trends of regional and monthly mean values, Deep Sea Res. Part 1, 86, 56-67, 2014.

460 Table 1: Correlation and partial correlation of SWH and MWP with DMI and NINO3 time
461 series during October from 1979 to 2014.

462

	Correlation with DMI		Partial correlation with DMI (ENSO removed)		Correlation with ENSO		Partial correlation with ENSO (DMI removed)	
	SWH	MWP	SWH	MWP	SWH	MWP	SWH	MWP
L1 (22ºN;67ºE)	-0.16	0.37	-0.19	0.23	-0.02	0.30	0.11	0.10
L2(19ºN;70.5ºE)	-0.27	0.48	-0.20	0.29	-0.19	0.45	0.03	0.20
L3(16.5ºN;71.5ºE)	-0.38	0.68	-0.31	0.51	-0.22	0.53	0.03	0.17
L4(13ºN;73ºE)	-0.56	0.69	-0.40	0.52	-0.46	0.59	-0.15	0.25
L5(10.5ºN;74.5ºE)	-0.59	0.57	-0.34	0.33	-0.59	0.60	-0.33	0.35
L6(7.5ºN;76ºE)	-0.59	0.55	-0.35	0.27	-0.56	0.61	-0.29	0.40

463

464

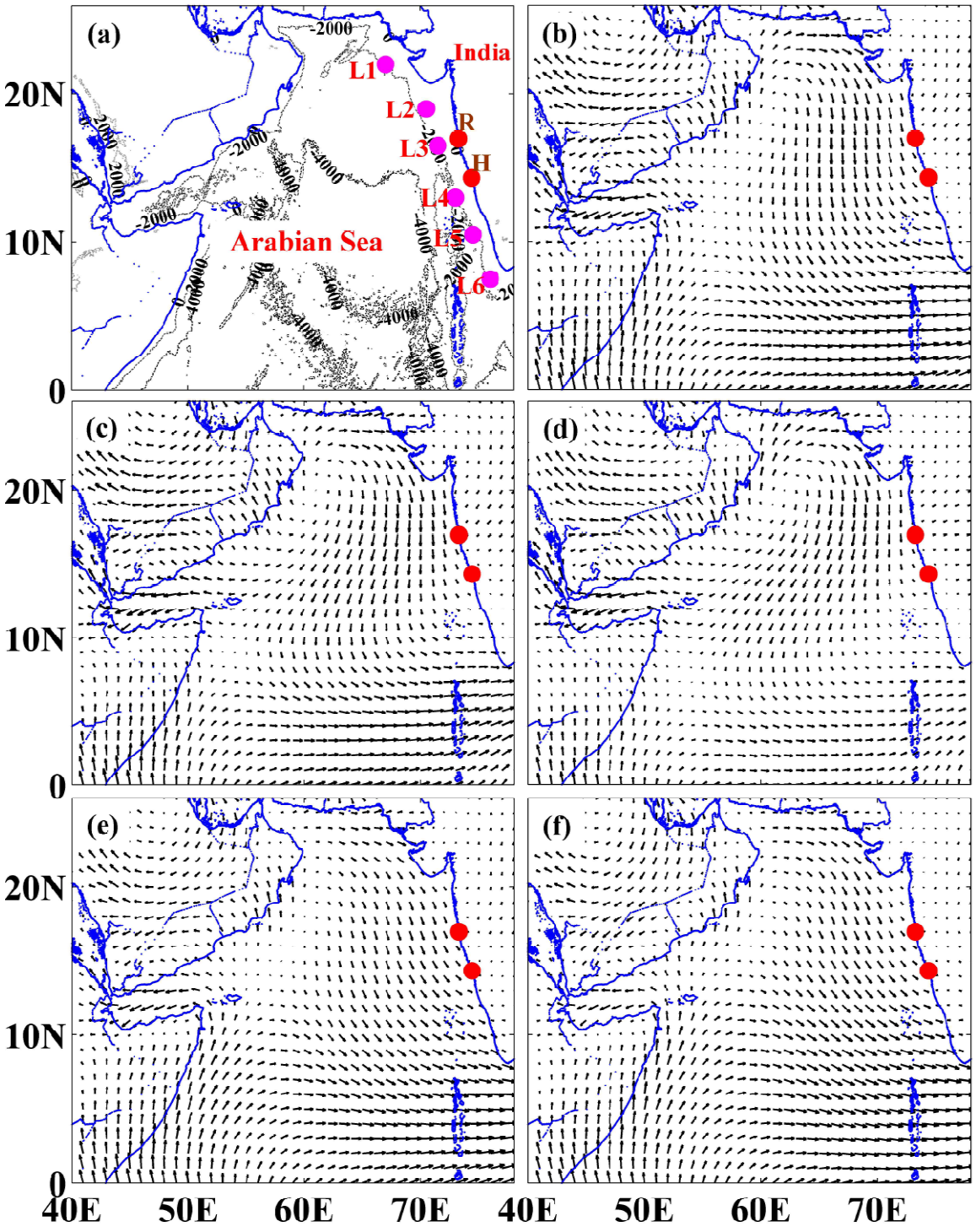

Figure 1: (a) The six locations considered to study the role of DMI on the wave climate are L1 to L6. The wave measuring locations (Ratnagiri and Honnavar) in central eastern AS are shown as red dots, b) Composite climatology of wind pattern during October in AS and part of equatorial Indian Ocean from 1958 to 2014. Averaged wind pattern during (c) pure positive IOD, (d) combined positive IOD, (e) Pure negative IOD and (f) Combined negative IOD from 1958 to 2014.

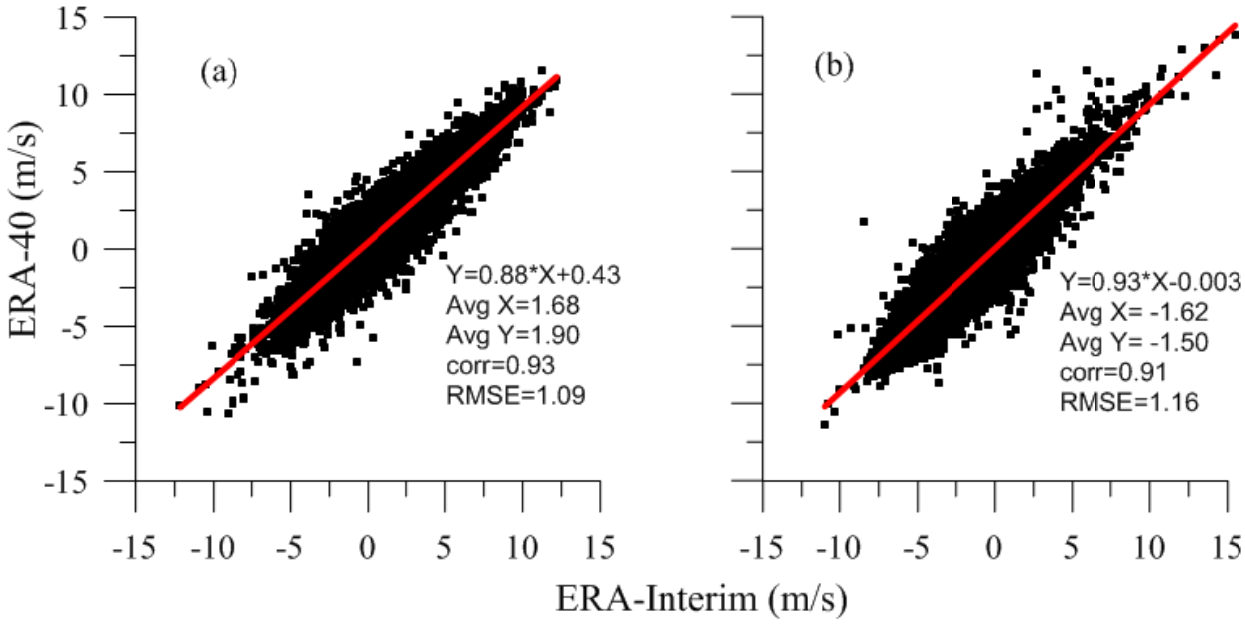

472

473 Figure 2 : Cross comparison of ERA-40 and ERA-I for October from 1979 to 2001. (a) zonal
474 wind (b) meridional wind

475

476

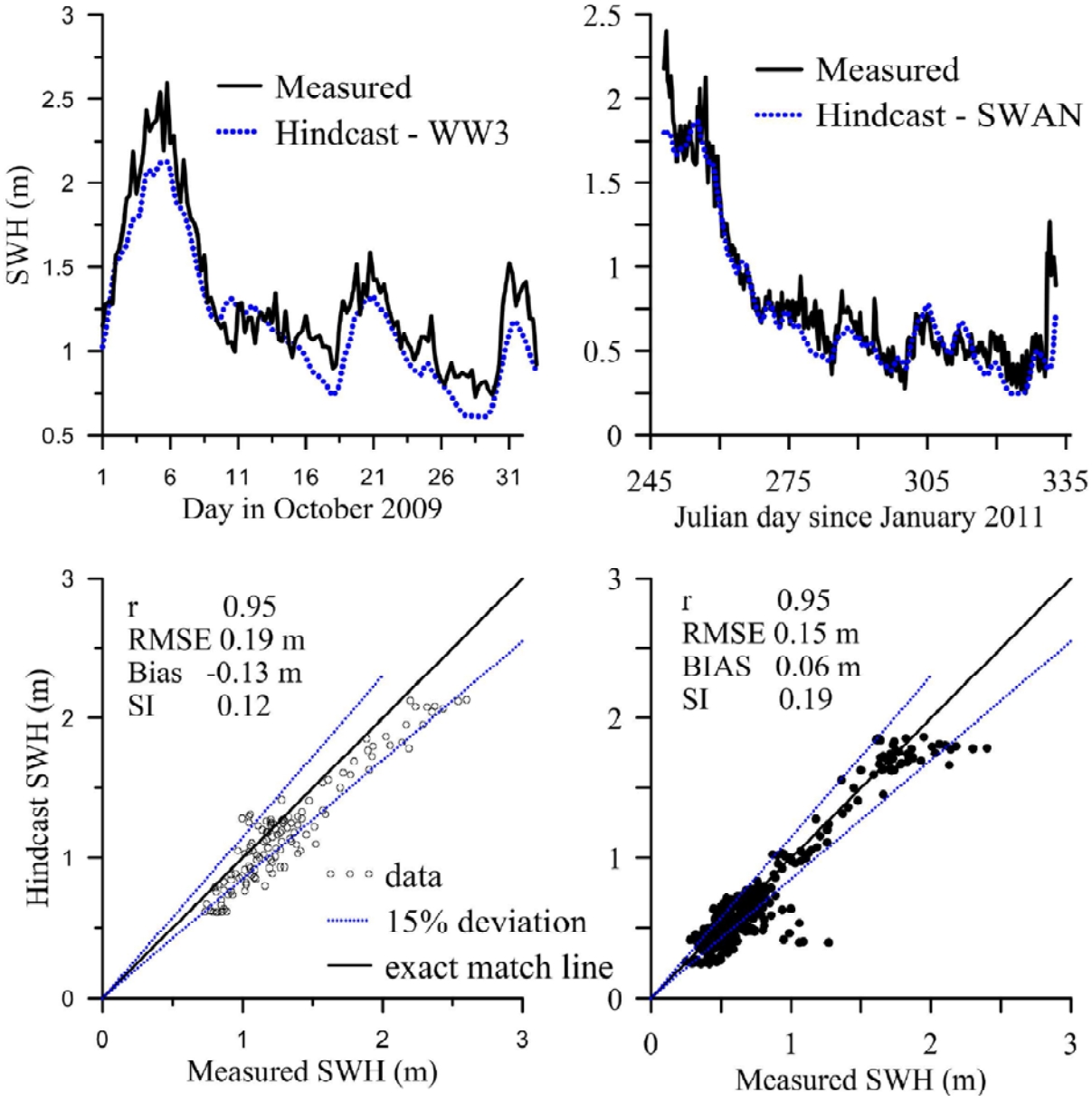

477

478 Figure 3: Comparison of hindcast SWH values with measured values. Left panel shows the
479 values during October 2009 at deep water location and the right panel shows the values
480 during September-November 2011 at shallow water location (Ratnagiri).

481

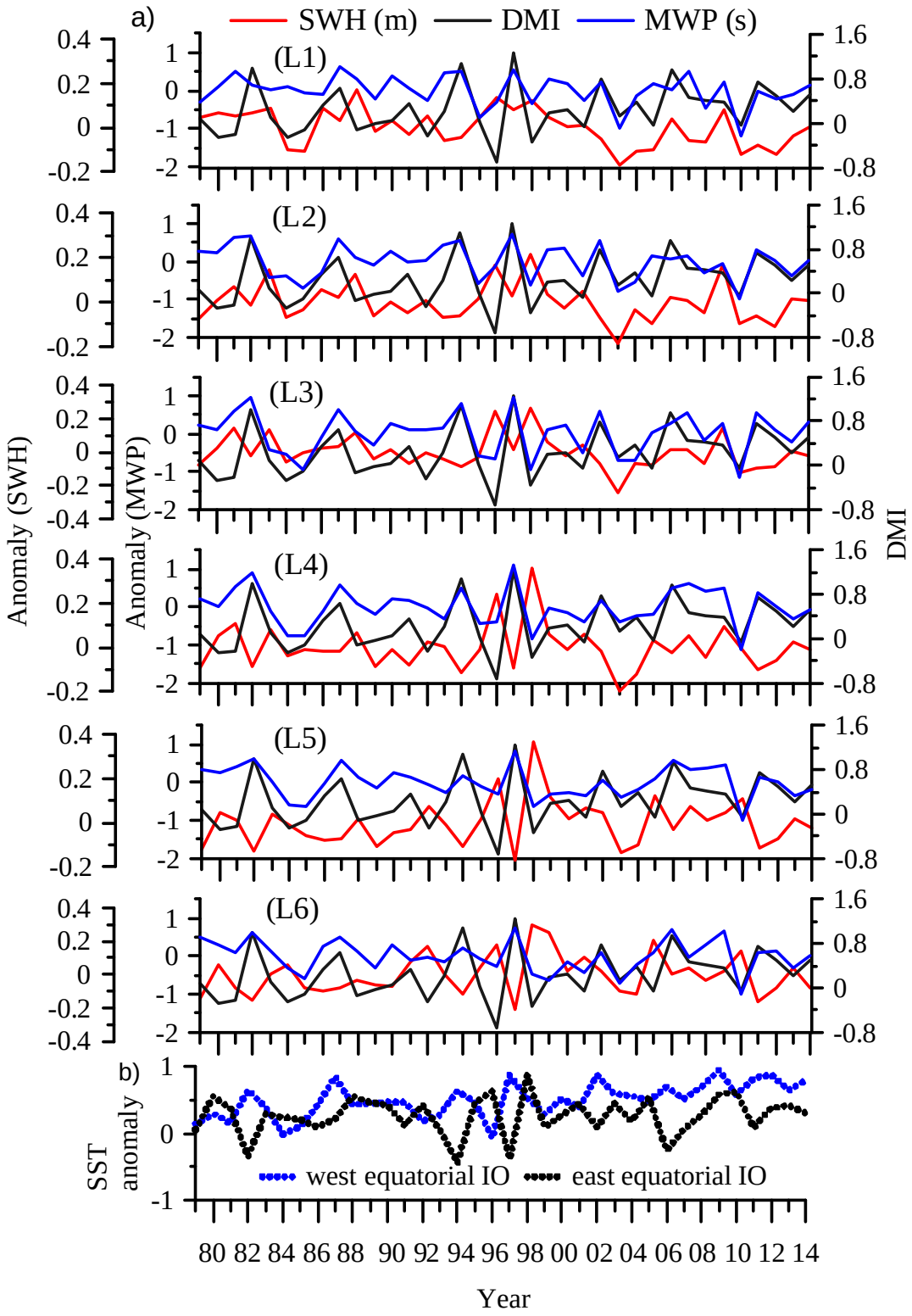

Figure 4 : a) Anomaly of significant wave height (SWH) and mean wave period (MWP) at selected six locations off west coast of India during October from 1979 to 2014 along with DMI. The wave data is from ERA-I. Locations are shown in Figure 1. b) Plot of SST anomaly in west and east equatorial IO. SST data is from Tropflux.

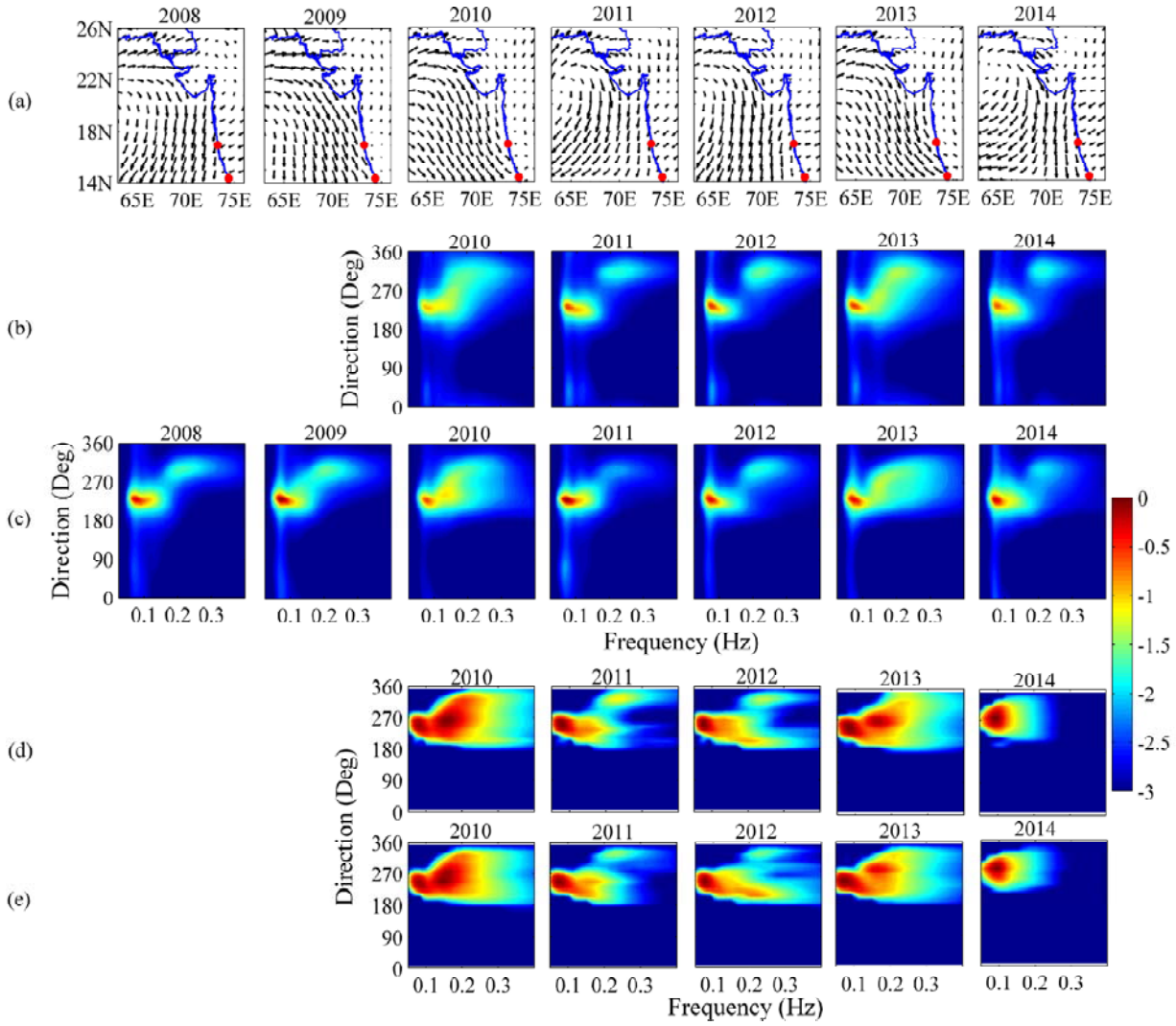

Figure5: Averaged wind pattern of October from 2008 to 2014 (row a). Averaged measured wave frequency-directional spectra from 2008 to 2014 off Ratnagiri (row b) and off Honnavar (row c) color bar is for spectral energy (m^2 *Deg/Hz) d) Modeled directional spectrum off Ratnagiri and (e) off Honnavar from 2010 to 2014. The spectral energy is shown in logarithmic scale base to 10. SST anomalies of eastern and western equatorial IO with DMI are shown in Figure 4.

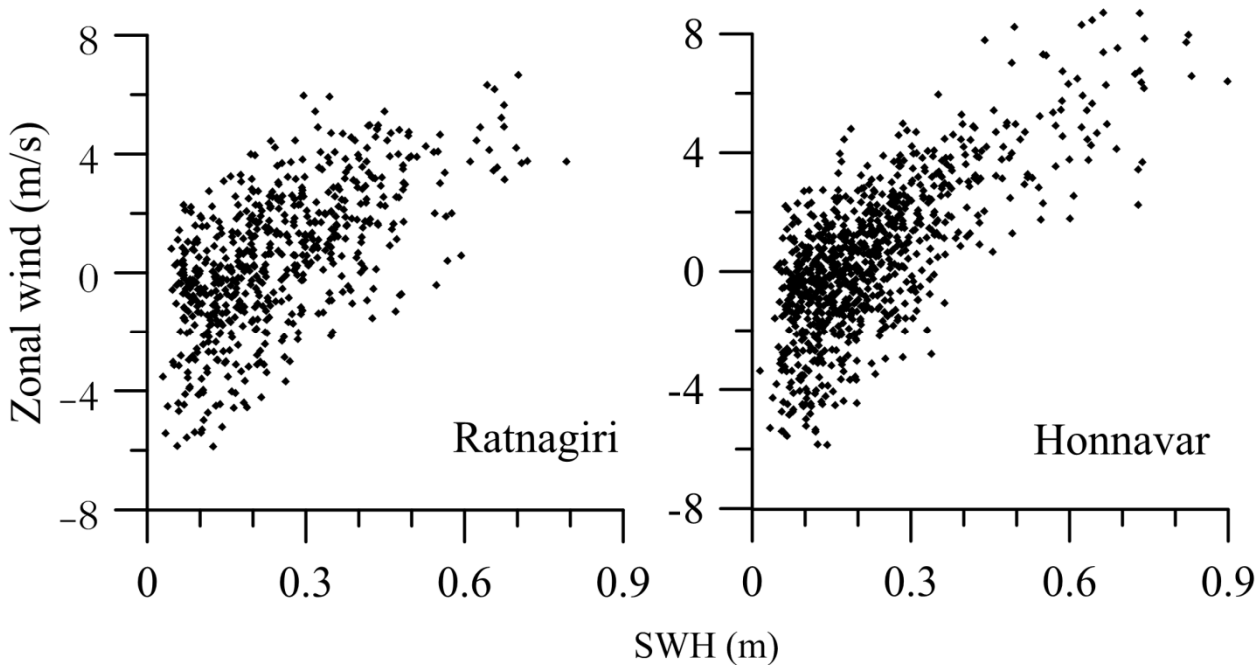

Figure 6 : Scatter plot of zonal wind within 14 N to 20 N and 70 E to 73 E with SWH of high frequency range (0.14 Hz to 0.29 Hz) and NW direction waves (280º to 320º) off Honnavar (from 2008 to 2014) and off Ratnagiri (from 2010 to 2014).

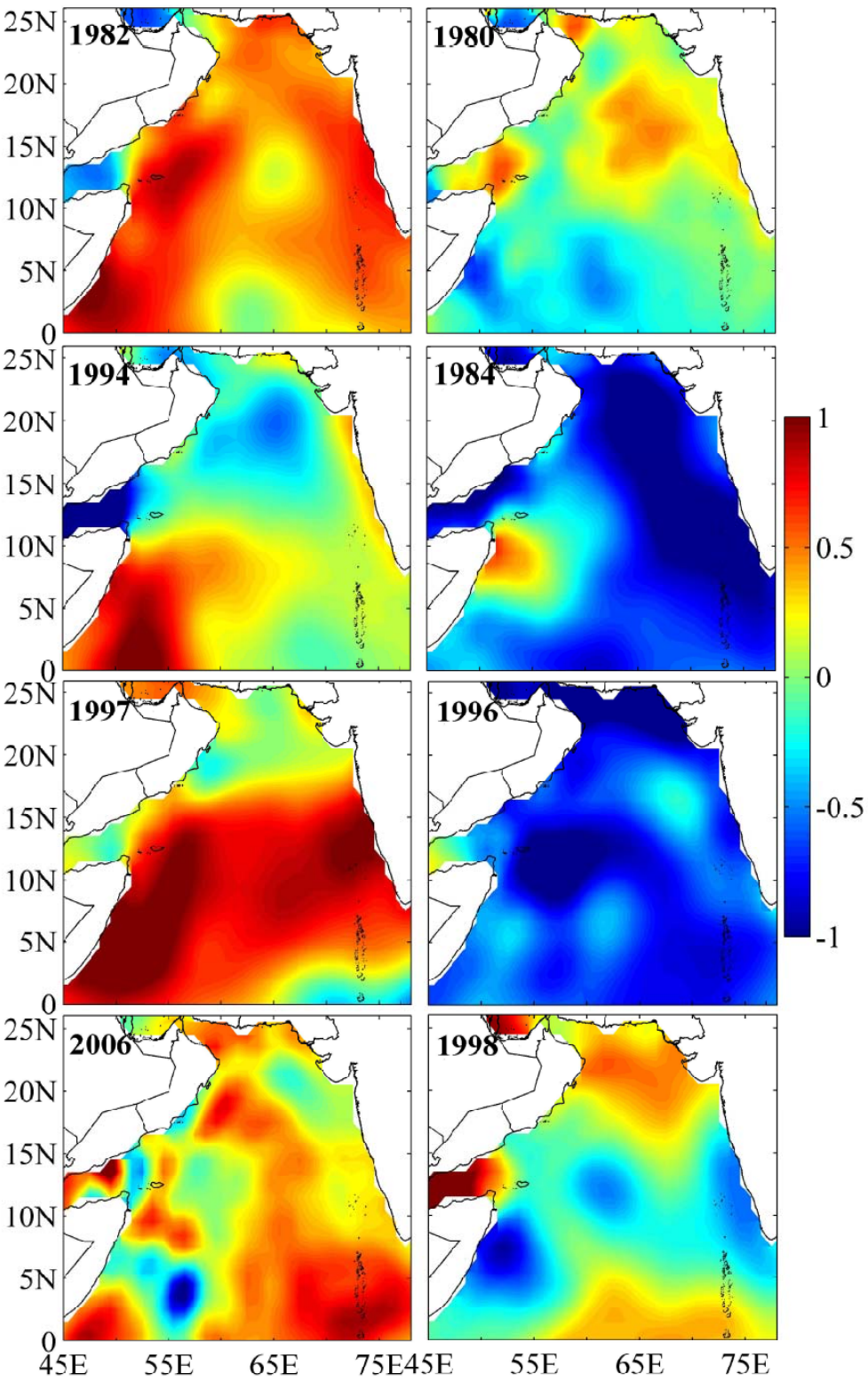

Figure 7: SST anomaly (ºC) of four strong positive (first column) and four negative (second column) IOD years from 1979 to 2014. Years are shown inside the figure and SST anomaly of eastern and western equatorial IO with DMI for corresponding years are shown in Figure 4.

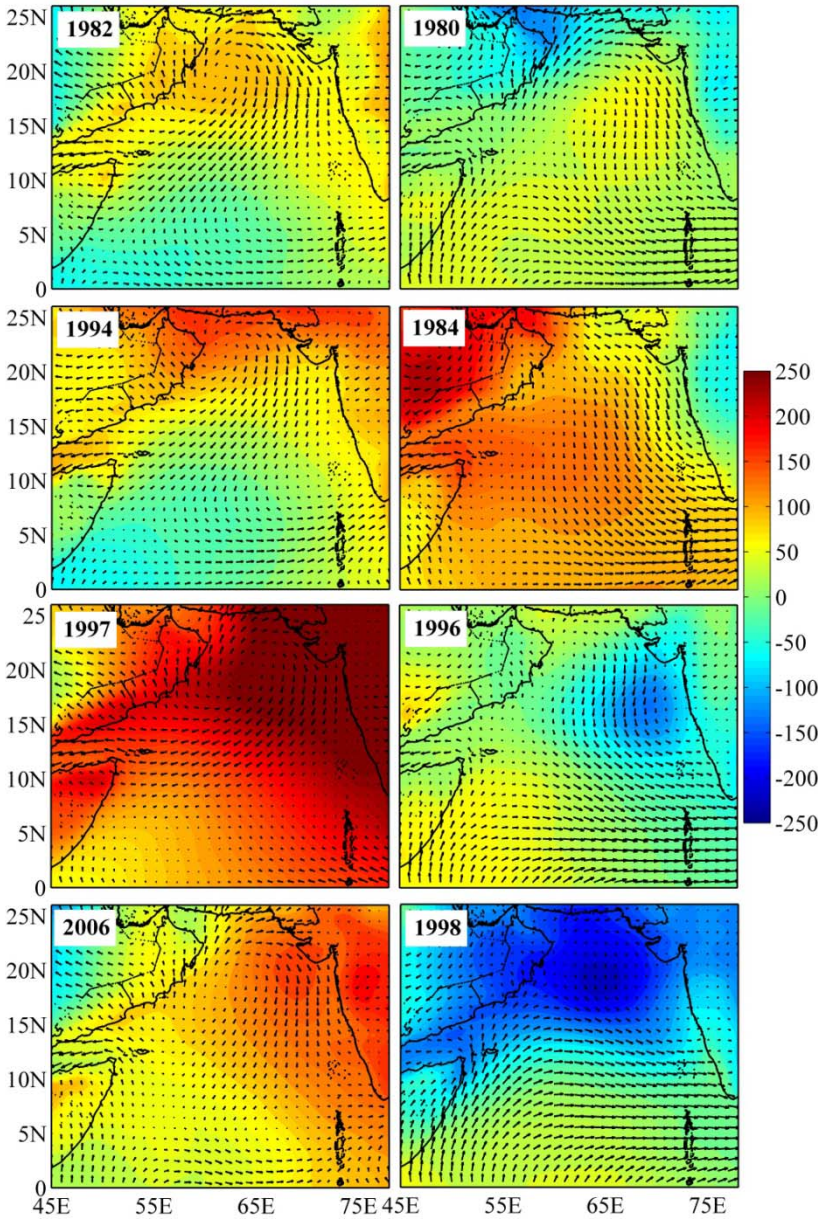

504

505 Figure 8: Wind vector (m/s) and SLP anomaly (Pa) of four strong positive (first column) and
506 four negative (second column) IOD years from 1979 to 2014. Years are shown inside the
507 figure and SST anomaly of eastern and western equatorial IO with DMI for corresponding
508 years are shown in Figure 4.

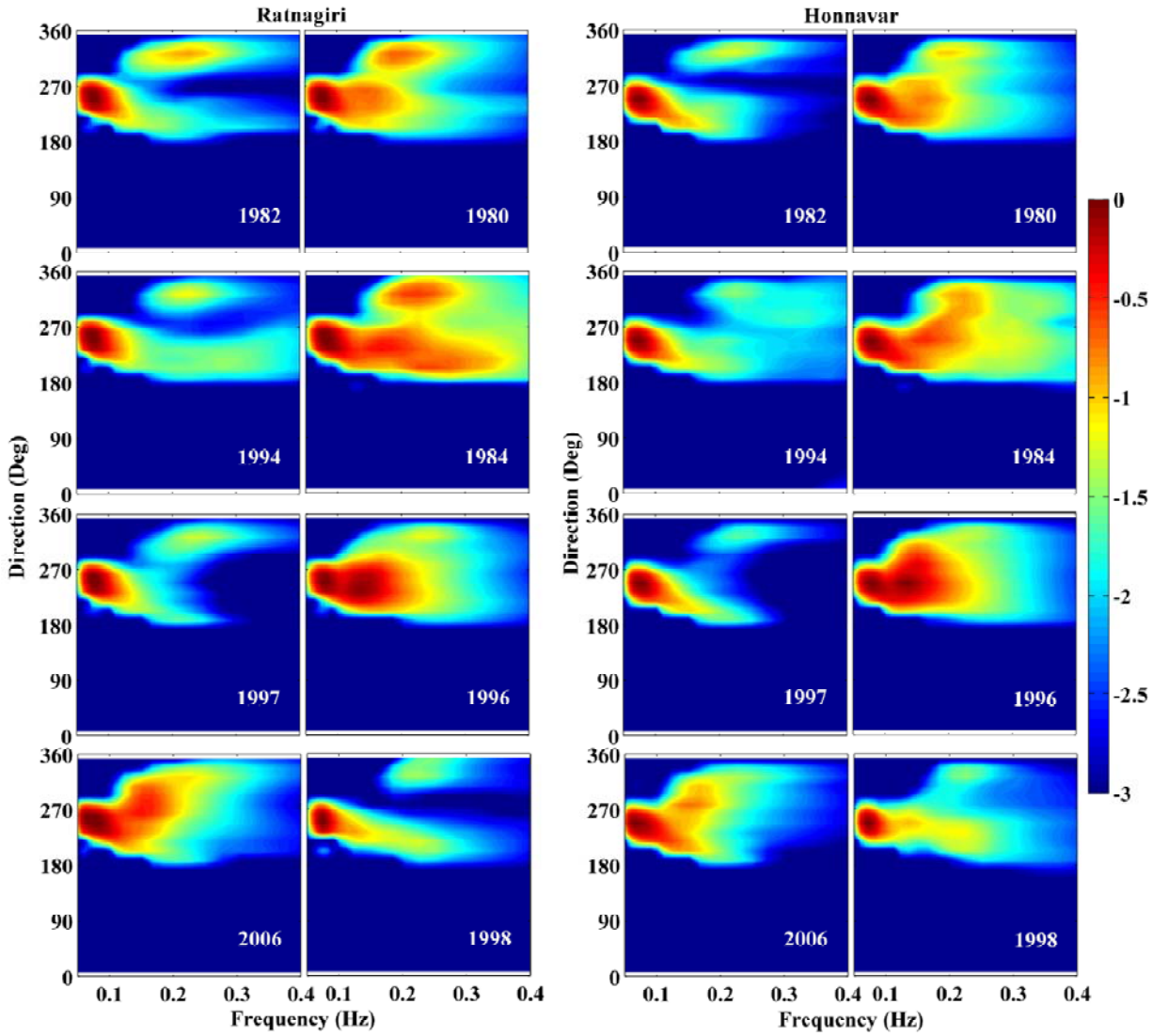

Figure 9: Modeled directional spectrum off Honnavar and Ratnagiri for selected positive and negative IOD years (columns one and three for positive IOD and two and four for negative IOD). Corresponding years are shown inside the figures and DMI are shown in Figure 4. The spectral energy is shown in logarithmic scale base to 10.